BIOCHEMISTRY
including biophysical chemistry & molecular biology

Article

pubs.acs.org/biochemistry

Effects of Macromolecular Crowding on Burst Phase Kinetics of Cytochrome *c* Folding

Eefei Chen,[†] Alexander Christiansen,[§] Qian Wang,[‡] Margaret S. Cheung,[‡] David S. Kliger,*[,†] and Pernilla Wittung-Stafshede*[,§]

[†]Department of Chemistry and Biochemistry, University of California, Santa Cruz, California 95064, United States

[‡]Department of Physics, University of Houston, Houston, Texas 77204, United States

[§]Department of Chemistry, Umeå University, 901 87 Umeå, Sweden

ABSTRACT: Excluded volume and viscosity effects of crowding agents that mimic crowded conditions in vivo on "classical" burst phase folding kinetics of cytochrome *c* are assessed in vitro. Upon electron transfer-triggered folding of reduced cytochrome *c*, far-UV time-resolved circular dichroism (TRCD) is used to monitor folding under different conditions. Earlier work has shown that folding of reduced cytochrome *c* from the guanidinium hydrochloride-induced unfolded ensemble in dilute phosphate buffer involves kinetic partitioning: one fraction of molecules folds rapidly, on a time scale identical to that of reduction, while the remaining population folds more slowly. In the presence of 220 mg/mL dextran 70, a synthetic macromolecular crowding agent that occupies space but does not interact with proteins, the population of the fast folding step for cytochrome *c* is greatly reduced. Increasing the viscosity with sucrose to the same microviscosity exhibited by the dextran solution showed no significant decrease in the amplitude of the fast-folding phase of cytochrome *c*. Experiments show that the unfolded-state heme ligation remains bis-His in the presence of dextran 70, but coarse-grained simulations suggest that the unfolded-state ensemble becomes more compact in the presence of crowders. We conclude that excluded volume effects alter unfolded cytochrome *c* such that access to fast-folding conformations is reduced.

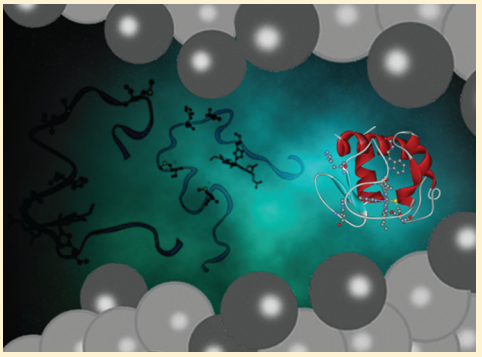

Through pioneering in vitro and in silico work over the past three decades, using, for example, protein engineering[1] and energy landscape theory,[2] significant progress has been made to pinpoint mechanisms and driving forces important for protein folding. In general, polypeptide folding is viewed as a random search of conformational space on a more or less rugged funnel-shaped energy surface that determines the number of intermediates populated during the folding process. However, in reality, proteins fold inside cells in which environments are very different from that of dilute buffer solutions most often used in experiments in vitro or modeled in silico. The intracellular environment is highly crowded because of the presence of large amounts of macromolecules, including proteins, nucleic acids, ribosomes, and carbohydrates. This means that a significant fraction of the intracellular space is not available to expanded macromolecular conformations. It has been estimated that the concentration of macromolecules in the cytoplasm ranges from 80 to 400 mg/mL.[3] All macromolecules in physiological fluids collectively occupy between 10 and 40% of the internal cellular volume.[4] The crowded environment results in increased viscosity, excluded volume effects, and the opportunity for specific, as well as nonspecific, intermolecular interactions. The question of how these effects, present when polypeptides normally fold in vivo, modulate protein folding reactions arises.

Because of excluded volume effects, any reaction that involves a volume change will be affected by macromolecular crowding.[5,6] It has been suggested that crowding provides a stabilizing effect to the folded states of proteins indirectly due to compaction of the more extended and malleable denatured states.[7,8] Macromolecular crowding can be mimicked experimentally by adding high concentrations of inert synthetic macromolecules, termed crowding agents, to the systems in vitro. Many in vitro experiments have shown increases in the stability of proteins in the presence of macromolecular crowding agents.[9−11] Less is known about the effects of macromolecular crowding on protein folding kinetics and mechanisms. While introduction of excluded volume will increase the driving force for folding, the viscosity is increased at high macromolecule concentrations, which may slow diffusion-dependent reactions. The microscopic spatial heterogeneity of a solution crowded with macromolecules results in macro- and microviscosities that differ in magnitude. Studies have shown that the microviscosity experienced by a protein during short time scale rotation or translation under crowded conditions is smaller than that measured for the bulk solution.[12,13]

Received: September 28, 2012
Revised: November 10, 2012
Published: November 12, 2012

ACS Publications © 2012 American Chemical Society

There have been in vitro crowding studies of protein dynamics on the nanosecond time scale[14,15] as well as on the millisecond to second time scales.[9,16] In addition, pioneering studies of protein folding inside living cells (on the second time scale) have been reported.[17] In this study, we bridge the time gap between nanoseconds and milliseconds using cytochrome *c* (cyt *c*) as our target system in vitro. To follow folding on the nanosecond to millisecond time scale, we use a nanosecond time-resolved circular dichroism (TRCD) approach developed in the Kliger lab.[18,19] Cytochrome *c* is an excellent model for studying the effects of crowding on protein folding because its fast folding kinetics have been extensively studied in dilute buffer solutions.[20] Understanding how cyt *c* folds in different crowded environments is also important because it is a key protein involved in electron transfer reactions in mitochondria,[21] as well as a signaling molecule for apoptosis in the cytoplasm.[22]

In this study, electron transfer-triggered folding experiments probed by TRCD demonstrate that there are changes in kinetic partitioning between the fast and slow folding phases of cyt *c* in the presence of 220 mg/mL dextran 70. Specifically, fast-folding conformations appear to be hindered, and most molecules fold on the millisecond time scale. To distinguish the viscosity effects versus excluded volume effects of dextran 70 on the TRCD results, we also studied the effects of sucrose on cyt *c* folding. TRLD measurements[23] of carbon monoxide-bound myoglobin (MbCO) were used to obtain protein rotational diffusion times and thus determine microviscosities under different solvent conditions. In vitro and in silico analyses of unfolded-state properties indicate no change in heme ligation but show there is overall compaction in the presence of the crowding agent.

EXPERIMENTAL PROCEDURES

Materials. Horse heart cytochrome *c*, horse skeletal myoglobin, NADH, all L-dextrans, and D-fructose (Sigma-Aldrich, St. Louis, MO), ultrapure guanidinium hydrochloride (GuHCl) (MP Biomedicals, Costa Mesa, CA), sodium phosphates (NaP, monobasic and dibasic) and L-sucrose (Thermo Fisher Scientific, Waltham, MA), and sodium hydrosulfite (dithionite) (Fluka Chemicals, Ronkonkoma, NY) were used without further purification.

Sample Preparation. For the far-UV TRCD studies of reduced cytochrome *c* (redcyt *c*) folding, buffer solutions (pH 7) were made by preparing two stock solutions for the two different folding experiments. The first stock solution contained 50 mM NaP with either 310 mg/mL sucrose or 220 mg/mL dextran 70, whereas the second stock solution contained 50 mM NaP, 6 M GuHCl, and either 310 mg/mL sucrose or 220 mg/mL dextran 70. The two stock solutions were mixed to obtain buffer solutions comprising either 4 M GuHCl, 50 mM NaP, and 220 mg/mL dextran 70 or 4 M GuHCl, 50 mM NaP, and 310 mg/mL sucrose. Solid oxidized cyt *c* (oxcyt *c*), solid NADH, and the buffer alone were separately deoxygenated with argon gas and then placed into a glovebag that was continuously purged with nitrogen gas. Once mixed, the final oxcyt *c* solutions (pH 7) contained ~50 μM protein and 400 μM NADH in either 4 M GuHCl, 50 mM NaP, and 220 mg/mL dextran 70 or 4 M GuHCl, 50 mM NaP, and 310 mg/mL sucrose. NaP is used throughout this work to refer to 50 mM NaP used in the TRCD studies presented here and to 0.1 M NaP used in the previously reported TRCD and time-resolved optical rotatory dispersion (TRORD) experiments.

For the TRLD experiments, buffer solutions (pH 7) containing 50 mM NaP, dextran 70 (50, 110, 150, 200, and 220 mg/mL), and sucrose (200, 340, 430, and 500 mg/mL) were prepared, added to a solution of myoglobin, and subsequently deoxygenated with CO gas. After ~30−45 min, sodium dithionite was added to form a solution of MbCO with absorption at 409 nm of approximately 0.8 in a 5 mm path length cuvette. Because cosolvents L-dextran and L-sucrose rotate the plane of polarized light, D-fructose was used as a compensator (or counter-rotator) (vide infra). The concentration of D-fructose required to counter-rotate the plane of polarized light was calculated using the equation $[\text{fructose}] = [\text{cosolvent}]([\alpha]_{D,\text{cosolvent}}/[\alpha]_{D,\text{fructose}})$. The specific optical rotation ($[\alpha]_D$) used for the dextrans was +198° and for L-sucrose +66.5° at 25 °C. If necessary, the final compensator solution was fine-tuned by either diluting or concentrating the solution until the MbCO LD baseline was zero. The specific rotation values cited above came from http://www.dextran.net and product specifications.

Cyt *c* samples (pH 7) for spectral equilibrium CD and magnetic CD (MCD) measurements were prepared in 50 mM NaP alone, 4 M GuHCl with 50 mM NaP, 6 M GuHCl with 50 mM NaP, 4 M GuHCl with 50 mM NaP and 310 mg/mL sucrose, and 4 M GuHCl with 50 mM NaP and 220 mg/mL dextran 70. The final concentrations were 20 μM for the oxcyt *c* solutions for measurements in the near- and far-UV regions and 42 μM for cyt *c* solutions for MCD data collection in the visible (450−650 nm) region. Samples of redcyt *c* were prepared by addition of sodium dithionite to oxidized cyt *c* solutions. The concentrations of the redcyt *c* samples were as described above for oxcyt *c*, except that for near-UV CD measurements ~70 μM protein was used.

GuHCl, dextran, and sucrose concentrations in the oxcyt *c* and MbCO samples and in the buffers for the TRCD, TRLD, and equilibrium CD and MCD measurements were determined from their refractive index values, which were measured on a refractometer (ABBE-3L, Milton Roy, Raleigh, NC). Adjustments of the pH to a final value of 7 were made with 0.1 M NaOH. The protein concentration and integrity of the protein before, during, and after all experiments were measured on a UV−vis spectrophotometer (UV-2102PC, Shimadzu, Columbia, MD). For dextran 70 solutions, the final concentration of GuHCl was corrected for the volume excluded to solvent because of the presence of the crowding agent, as described previously.[24,25]

Time-Resolved Circular Dichroism Experiments. Rapid oxidation of NADH, and subsequent electron transfer to oxcyt *c*, was triggered by absorption of a 355 nm photon from a Quanta-Ray PRO-250-10 pulsed Nd:YAG laser. The rapid reduction of oxcyt *c* triggered protein folding, which was followed spectrally as a function of time using TRCD spectroscopy. The basic design of the TRCD instrument has been detailed previously[18,19] and is discussed here only briefly. A xenon flash lamp probe beam was passed through a MgF_2 polarizer, a strain plate to produce left and then right elliptically polarized light, and then a telescope, which focused the beam diameter to ~1 mm at the sample. This modification of the probe beam allows for experiments on small sample volumes. The initially 9 mm diameter laser beam [~23 mJ, 7 ns (full width at half-maximum)] was focused to a spot size of ~2 mm to overlap with the probe beam at the sample. After passing through a second MgF_2 polarizer, the probe beam was collected by a spectrograph and detected by a CCD.

On the TRCD apparatus, the cross position of the two polarizers is determined in the presence of buffer, which is typically sodium phosphate. However, because sucrose and dextran rotate the plane of polarized light, measurements at that cross position lead to significant attenuation of the CD signal compared with that measured in buffer alone. This problem can be addressed in two ways. The first approach is by using a solution to compensate for the rotation of light, and the second is by redefining the cross position using, in this situation, either dextran 70 or sucrose. Both methods allow recovery of the CD signal, and the latter was used for these TRCD experiments.

For the TRCD measurements, the deoxygenated oxcyt *c* samples were maintained under a positive nitrogen atmosphere in a glovebag, which also contained a peristaltic pump to pass oxcyt *c* to a 0.5 mm path length cell that was constructed with fused silica windows. TRCD data were collected 550 and 630 ns, 1, 2, 10, 50, 100, and 500 μs, and 1, 10, 50, and 100 ms after the initial photoreduction event for redcyt *c* folding in 4 M GuHCl, 50 mM NaP, and 220 mg/mL dextran 70. For folding in 4 M GuHCl, 50 mM NaP, and 310 mg/mL sucrose, data were measured 550 and 630 ns, 1, 2, 20, 32, 50, 100, and 500 μs, and 1, 5, 10, 50, and 100 ms after photoinitiation of the reaction. The time points were chosen to focus on the fast (burst) phase of folding rather than the slow phase. The TRCD results represent 208−344 and 252−440 averages for the sucrose and dextran experiments, respectively. TRCD measurements were collected with a 2 s delay between each laser flash for experiments with redcyt *c* folding in 310 mg/mL sucrose and with a 10 s delay for folding in 220 mg/mL dextran 70. The sample flowed only between laser shots at a flow rate of 9 μL/s. Flow at this rate was designed to prevent buildup of photoproduct or photodegraded products. After irradiation, the sample flowed out to a collection vial in the glovebag. The integrity of the sample was evaluated for the buildup of redcyt *c* by absorption measurements. The sample was maintained at a temperature of 21 °C, and the temperature was checked periodically throughout the experiments.

Time-Resolved Linear Dichroism Experiments. The rotational diffusion time for myoglobin can be determined by photolyzing a heme-bound CO ligand with linearly polarized laser light (at 532 nm) and monitoring the time dependence of the resulting deoxymyoglobin linear dichroism. Specifically, polarized excitation of an isotropic protein sample will result in preferential excitation of molecules with aligned transition dipoles, forming an oriented subset. Because there is a difference in the extinction coefficient of the photoproduct (deoxymyoglobin) and of the initial species (MbCO), the sample will be linearly dichroic. With time, the photoselected population undergoes reorientation because of rotational diffusion and the polarization anisotropy decays to zero.

The design of the ultrasensitive TRLD approach[23] is very similar to that of the TRCD instrument. However, the TRLD apparatus uses two Glan-Taylor polarizers, positioned around the sample, that are oriented at ±45° relative to the vertical laser polarization (with laser and probe beams passing through the sample at 90° to each other). To compensate for the rotation of the plane of polarized light, a counter-rotator solution was positioned after the sample, but before the second, analyzing polarizer. LD intensities are measured by rotating the analyzing polarizer by $\pm\beta$ (5° for these experiments) off the crossed position of the two polarizers. The LD signal is the difference divided by the sum of the intensities measured when the analyzing polarizer is positioned at $\pm\beta$.

TRLD data for MbCO were measured at 12−27 time points (with a detector gate of 5 ns) between 2.5 ns and 10 μs after photolysis of the CO ligand, which was initiated with a frequency-doubled Quanta Ray DCR-2A Nd:YAG laser [532 nm, 7 ns pulse width (full width at half-maximum)]. The repetition rate was 2 Hz, and the laser energy was ∼23 mJ/pulse. One hundred averages were measured at each time delay for each data set, and on average under each different cosolvent condition seven sets of data were obtained. The temperature of the sample was maintained at 21 °C during the experiments.

Equilibrium CD and MCD Spectral Experiments. Far- and near-UV CD spectra of oxcyt *c* and redcyt *c* were measured on a CD spectrophotometer (model 62DS, AVIV, Lakewood, NJ). With the addition of a 0.64 T PM-2 permanent magnet (JASCO Inc., Easton, MD), visible MCD spectra were also collected for cyt *c* in the solutions described above. Spectra were obtained using 1, 10, and 5 mm path length quartz cells in the spectral regions from 200 to 300 nm, from 240 to 340 nm, and from 450 to 650 nm, respectively. Three to seven sets of data for each sample were collected every 1 nm with a 1 nm bandwidth using an integration time of 4 or 8 s. For MCD experiments, data were collected for two different orientations of the magnetic field, parallel and antiparallel to the propagation direction of the light beam. The MCD spectra were calculated from the difference in the signals in parallel and antiparallel orientations divided by 2. MCD data were compared in the 450−520 nm range because this region is diagnostic of the heme ligand coordination for oxcyt *c*.[26,27] Thus, differences in the heme ligation state between the folded and unfolded forms of oxcyt*c* are best observed in this spectral region.

Experimental Data Analysis. TRCD and TRLD data are presented and analyzed as multiwavelength difference spectra calculated by subtracting the initial oxcyt *c* or MbCO spectra from the time-resolved spectra. Kinetic CD signals were obtained by averaging the spectral data over the 220−224 nm range. The fractional secondary structure formation was calculated using the difference CD signals measured at each time delay relative to the difference CD signal between the final folded (redcyt *c*) protein and the oxidized starting material. Singular-value decomposition (SVD), global kinetic, and exponential fitting analyses were performed on the TRCD and TRLD data using Matlab (The MathWorks, Inc., South Natick, MA).

Coarse-Grained Simulations. A side chain C_α model[28] (SCM) that includes two beads per amino acid (except glycine) was used to represent the structure of cyt *c*. We started from our previous model of cyt *c* (including the heme),[24] which is a variant of another model developed by the Wolynes group,[29] and built a structure-based Hamiltonian with additional modifications that included the formation of non-native bis-His coordination as follows. To investigate the probability of non-native bis-His formation, a Lennard-Jones (LJ) potential was used between the heme and His26/His33 in replacement of repulsion in our previous work.[24] The LJ potential between heme and His26/His33 is given in eq 1: i is the side chain bead of His26/His33, and $j \in H_m$ (m = 1, 2, 3, or 4), which are the four beads representing the heme

$$E^{ij} = \varepsilon\left[\left(\frac{\sigma_{ij}}{r_{ij}}\right)^{12} - 2\left(\frac{\sigma_{ij}}{r_{ij}}\right)^{6}\right] \quad (1)$$

where ε = 2.4 kcal/mol, $\sigma_{ij} = f(\sigma_i + \sigma_j)$, f = 0.9, and σ_i and σ_j are the van der Waals radii of the interacting beads. Formation of non-native bis-His coordination was confirmed upon satisfying the following two conditions: (1) the distance from the side chain bead of His26/His33 to any bead of heme should be less than 5.2 Å, and (2) the side chain bead of His18 and the side chain bead of His26/His33 should be on the different sides of the heme plane. The coarse-grained model of dextran 70 was the same as in our previous work.[24] In short, dextran was modeled as two hard spheres linked by a harmonic bond whose equilibration length is 83.6 Å. The radius of each hard sphere is 41.8 Å. There are only repulsive interactions between crowder and crowder and between crowder and protein. The volume fraction (φ_c) used was 40%.

To study in silico thermodynamic properties of cyt *c*, molecular simulations using Langevin equations of motion in the low-friction limit were employed.[30] An in-house developed version of AMBER10 was used. The Replica Exchange Method (REM)[31] was implemented to enhance the sampling efficiency. The integration time step is $10^{-3}\tau_L$, where $\tau_L = (m\sigma^2/\varepsilon)^{0.5}$, where m is the mass of a C_α bead, ε is the solvent-mediated interaction, and σ is the van der Waals radius of a C_α bead. Each exchange was attempted every $400\tau_L$. For the computations of thermodynamic values, a total number of at least 40000 statistically significant conformations were collected from each replica. Error analysis was estimated by the jackknife approach.

RESULTS

Because of redox-dependent stability, there are intermediate GuHCl concentrations at which oxcyt *c* is unfolded and redcyt *c* is folded.[32,33] Here, 4 M GuHCl was used for the experiments because a large burst phase amplitude was detected in previous TRCD studies of redcyt *c* folding in buffer at this denaturant concentration.[34] To create a crowded condition, we used 220 mg/mL dextran 70. Dextran is an inert crowding agent that occupies space but does not interact with proteins.[35] The concentration of 220 mg/mL was selected as a relevant in vivo concentration.

To first characterize possible equilibrium effects of 220 mg/mL dextran 70 on cyt *c* in 4 M GuHCl, the secondary and tertiary structures of oxcyt *c* and redcyt *c* were explored using far- and near-UV CD spectroscopy. Figure 1A shows the far-UV spectra of oxcyt *c* and redcyt *c* in 4 M GuHCl, 50 mM NaP, and 220 mg/mL dextran 70. The oxcyt *c* spectrum is compared to and overlays well with the spectrum of oxcyt *c* unfolded with 4 M GuHCl and 50 mM NaP. However, the spectrum of redcyt *c* in dextran 70 remains folded, as demonstrated by its comparison with that of redcyt *c* measured in 50 mM NaP and in 50 mM NaP with 4 M GuHCl. In Figure 1B, the near-UV CD spectrum of oxcyt *c* in 4 M GuHCl, 50 mM NaP, and 220 mg/mL dextran 70 is comparable to the spectrum of unfolded oxcyt *c* (4 M GuHCl and 50 mM NaP) and quite different from that of folded oxcyt *c* (50 mM NaP). On the basis of these data, we conclude that the presence of 220 mg/mL dextran 70 does not alter the denatured state in terms of CD spectral characteristics reporting on secondary structure content. This was earlier concluded for thermally denatured cyt *c* in the presence of dextrans.[24] Dextran 70 also does not perturb the denatured tertiary structure of oxcyt *c* or the native, folded

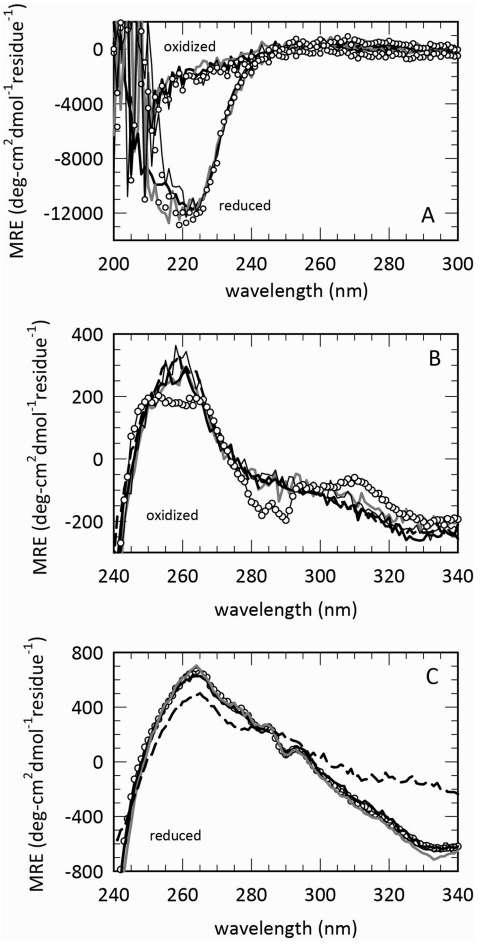

Figure 1. Equilibrium CD data. (A) Equilibrium far-UV CD spectra of oxcyt *c*, unfolded in 4 M GuHCl and NaP (thick black line) with 220 mg/mL dextran 70 (gray line), with 310 mg/mL sucrose (thin black line), and without crowder (black line, ○) measured in a 1 mm path length cell. In these same buffers (with and without crowders), the far-UV CD spectra of redcyt *c* are folded. (B) Equilibrium near-UV CD spectra of unfolded oxcyt *c* in 4 M GuHCl and NaP (thick black line) with 220 mg/mL dextran 70 (gray line), with 310 mg/mL sucrose (thin black line), and folded, without crowder (black line, ○), measured in a 10 mm path length cell. (C) Equilibrium near-UV CD spectra of folded redcyt *c* in 50 mM NaP (black line, ○), 4 M GuHCl and NaP (thick black line), 4 M GuHCl, NaP, and 220 mg/mL dextran 70 (gray line), and 4 M GuHCl, NaP, and 310 mg/mL sucrose (thin black line). These spectra are compared to that of the unfolded structure of redcyt *c* measured in 6 M GuHCl and NaP (dashed line).

secondary and tertiary structures of the redcyt *c* protein. Figure 1C shows that the near-UV CD spectra for redcyt *c* in 4 M GuHCl, 50 mM NaP, and 220 mg/mL dextran 70 overlay closely with the spectra for redcyt *c* in 50 mM NaP and 50 mM NaP with 4 M GuHCl (folded), but not with the spectrum measured in 50 mM NaP and 6 M GuHCl (unfolded).

To probe the effect of dextran 70 on the heme ligation state of the oxidized and reduced proteins, MCD spectroscopy was used. For oxcyt *c*, spectral measurements were focused in the region of 450−520 nm, which is sensitive to differences in the heme coordination between the unfolded and folded states.[26,27] Figure 2A shows that the MCD spectrum of oxcyt *c* in 4 M GuHCl, 50 mM NaP, and 220 mg/mL dextran 70 reflects the unfolded, His−Fe−His, heme ligation (50 mM NaP and 4 M GuHCl) rather than that of the folded, Met−Fe−His, heme

dx.doi.org/10.1021/bi301324y | *Biochemistry* 2012, 51, 9836−9845

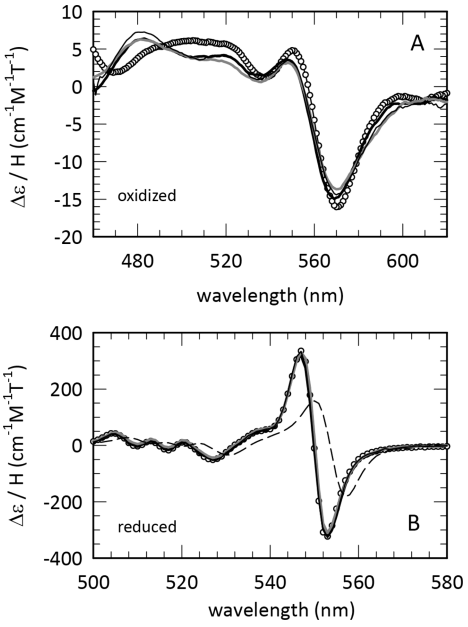

Figure 2. Equilibrium MCD spectra of oxcyt *c* and redcyt *c*. (A) The MCD spectra of oxcyt *c* in 4 M GuHCl and NaP (thick black line), 4 M GuHCl, NaP, and 220 mg/mL dextran 70 (gray line), and 4 M GuHCl, NaP, and 310 mg/mL sucrose (thin black line) overlay well. They are distinct from the spectrum of folded oxcyt *c* in 50 mM NaP (black line, ○). (B) Unlike the MCD spectrum of redcyt *c* in 6 M GuHCl and NaP (unfolded, dashed line), the spectra obtained in 4 M GuHCl and NaP (thick black line), 4 M GuHCl, NaP, and 220 mg/mL dextran 70 (gray line), 4 M GuHCl, NaP, and 310 mg/mL sucrose (thin black line), and 50 mM NaP (black line, ○) reflect the heme coordination found in the native, folded protein.

coordination (50 mM NaP). In contrast, Figure 2B shows that the spectrum of redcyt *c* in 4 M GuHCl, 50 mM NaP, and 220 mg/mL dextran 70 has a heme ligation state that is similar to that for folded redcyt *c* in 50 mM NaP and in 50 mM NaP with 4 M GuHCl. In summary, the results of the equilibrium far- and near-UV CD and MCD measurements provide the structural background for understanding the initial and final states involved in the far-UV TRCD experiments described below.

Electron injection from 355 nm laser excitation of NADH into unfolded oxcyt *c* in 4 M GuHCl and NaP triggers folding of the reduced form.[32,33,36] That is, upon the rapid transfer of an electron to the initially unfolded oxidized protein, which comprises a His−Fe(III)−His heme coordination, the immediate photoproduct is the unfolded reduced protein. However, because the reduced protein favors the folded conformation with a His−Fe(II)−Met heme ligation, folding is triggered. The reaction is probed by TRCD spectroscopy using a quasi-null ellipsometric approach that allows for nanosecond time resolution. Earlier work using this method revealed that folding of redcyt *c* under dilute conditions is complex, with a fraction of unfolded molecules folding as fast as the actual reduction step (fast phase, <1 ms), whereas the rest folded on the millisecond time scale (slow phase, >1 ms).[34,36] Similar to suggestions made for folding of cytochrome *c*′,[37] we proposed that heterogeneity in the unfolded ensemble of redcyt *c* resulted in kinetic partitioning between fast and slow phases. The heterogeneity was suggested to arise from slow conformational diffusion of the unfolded chains such that in the fast-folding phase near-native structure formation is produced in a subset of chain conformers rather than partial folding throughout the bulk of the sample. This formation of a molten globule-like intermediate is supported by studies of horse heart cyt *c* in the presence of sodium dodecyl sulfate,[38] as well as the observation of a faster time constant at higher denaturant concentration in microsecond molecular collapse experiments.[39] Here we have repeated this experiment in the presence of 220 mg/mL dextran 70 and collected far-UV CD spectra at time points between 500 ns and 0.1 s after the initiation of folding. Complementary time-resolved absorption (TROD) experiments indicate that under these conditions, the multiphase electron transfer reaction begins with a fast, ∼100 ns, process and reaches completion within 100 μs, similar to reduction times found previously without dextran 70.[34,36]

Our earlier data for the burst phase in redcyt *c* folding[34,36] were obtained from both nanosecond TRCD and TRORD measurements. Because TRORD and TRCD both probe secondary structure changes, these methods are expected to report on the same molecular processes in folding. Indeed, the 2003 study[34] showed that the time evolution of redcyt *c* folding in 3.3 M GuHCl using TRORD detection closely matched the kinetics that was measured in 1999 using TRCD.[36]

In Figure 3A, we compare the data for ET-triggered folding of redcyt *c* in the presence of 220 mg/mL dextran 70 with that

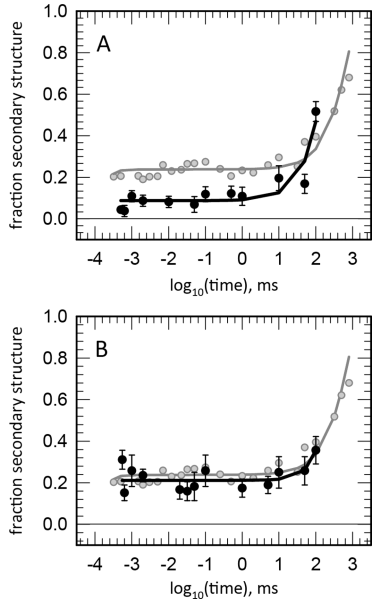

Figure 3. Time-resolved CD data. (A) Fraction of secondary structure formed as a function of time for redcyt *c* folding in 4 M GuHCl and NaP without (gray circles) and with (black circles) 220 mg/mL dextran 70. The gray line represents the fit to the kinetic data for redcyt *c* in 4 M GuHCl and NaP.[34] Within 550 ns, ∼10% secondary structure is formed. (B) Fraction of secondary structure formed as a function of time for redcyt *c* folding in 4 M GuHCl and NaP without (the gray line represents the fit to the data; data points are shown as gray circles) and with 310 mg/mL sucrose (black circles). Approximately 20% secondary structure is formed within 550 ns. The black lines represent the fits to the data measured in sucrose and dextran.

previously measured in buffer, both at 4 M GuHCl. The folding kinetics of redcyt *c* in 4 M GuHCl and NaP involves a fast phase comprising ∼20% of the total far-UV CD change and a slow millisecond phase (τ = 380 ms).[34] In contrast, folding in the presence of 220 mg/mL dextran 70 and 4 M GuHCl is dominated by the slow folding phase and there is a decrease

dx.doi.org/10.1021/bi301324y | *Biochemistry* 2012, 51, 9836−9845

from 0.24 to 0.1 in the fraction of secondary structure formed in <1 ms. That is, the level of formation of secondary structure associated with the fast-folding phase, observed to form in <0.4 μs, is significantly reduced in the dextran 70 sample. The kinetics on time scales longer than 1 ms (slow folding phase) are not analyzed here because the focus of this study is the burst kinetics and our experimental conditions are not optimized for longer time scales.

The changes observed in the redcyt *c* folding kinetics upon addition of dextran 70 are likely due to an excluded volume effect but could also be due to the increased viscosity that comes with the crowding agent. Increased viscosity should slow dynamics but not affect kinetic partitioning between paths or unfolded-state properties. However, increased viscosity may affect conformational dynamics within the unfolded ensemble such that fast-folding conformations are not as accessible. To assess the role of viscosity, we introduced sucrose into the redcyt *c* sample at a concentration that exhibits the same microviscosity as dextran 70.

To determine the microviscosity of 220 mg/mL dextran 70 that a protein experiences, we turned to TRLD experiments on CO-complexed myoglobin (MbCO). Myoglobin was selected because its reorientation through rotational diffusion occurs on distance and time scales that are close to those expected for early redcyt *c* folding events. Figure 4A compares the kinetics following photolysis of MbCO in 340 mg/mL sucrose obtained from TRLD and TROD spectroscopy. With a plot of the peak-to-trough amplitudes as a function of time, it is clear that the TRLD signal (reporting on rotational diffusion) decays to zero (τ = 68 ns), whereas the TROD signal (reporting on rebinding of CO to Mb) remains constant. This result demonstrates that, indeed, TRLD reports on the rotational diffusion dynamics of the protein and does not reflect the chemistry of CO recombination.

In Figure 4B, we show the rotational diffusion times measured for myoglobin in various concentrations of dextran 70 and sucrose as a function of bulk viscosity. The TRLD data were best fit to two exponential processes. The first exponential lifetime was not affected by the concentration, the molecular weight, or the size of the cosolvent and was assigned to distortion of the earliest LD data because the laser pulse extends over several nanoseconds. On the basis of more than 90 experiments, the time constant for this process is 4.8 ± 0.5 ns. The second exponential process is attributed to the rotational diffusion of MbCO after photolysis.

When we compared the rotational diffusion times for myoglobin in 220 mg/mL dextrans of different sizes (6−70 kDa), we found that the times are very similar (data not shown). This implies that the protein-containing cavities present in all these dextran solutions are large enough for myoglobin to undergo rotation without coming in constant contact with the dextran polymer chains. In agreement, when using fluorescent correlation spectroscopy and calmodulin labeled with green fluorescent protein as the probe, translational diffusion was found to vary only 2-fold between dextran 10 and dextran 70.[40]

The rotational diffusion times in dextran 70 for myoglobin can be related to microviscosities by extrapolating the measured time constants back to the sucrose data (in which micro- and macroviscosity are the same). We find that in the presence of 220 mg/mL dextran 70, the microviscosity is ∼3-fold higher than in water. The lower effective viscosity (as compared to the bulk viscosity, which is 60-fold higher than in water) is similar

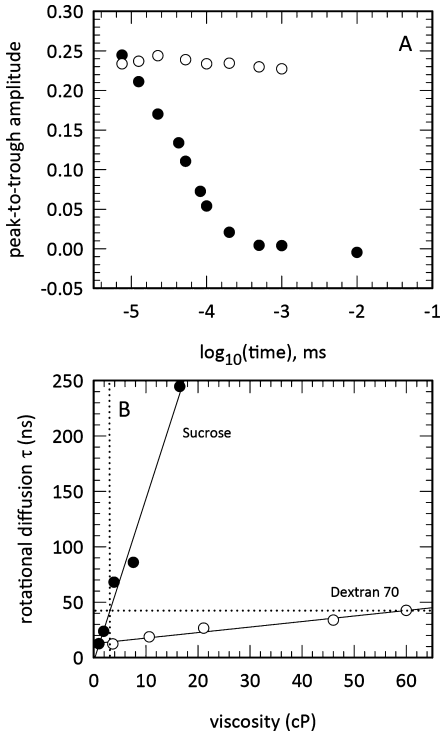

Figure 4. Time-resolved LD data. (A) Comparison of the peak-to-trough amplitudes for TROD (○) and TRLD (●) data as function of time following photolysis of MbCO in 340 mg/mL sucrose. As the TRLD signal returns to zero, the TROD signal remains constant. (We note that it would have been ideal to use cyt *c* for these TRLD experiments; however, an equivalent photolysis trigger is not available for the folded protein. Only when the protein is unfolded is it possible for cyt *c* to bind CO. This poses a potential problem for the TRLD measurements because rotational diffusion is likely to proceed in parallel with protein folding, which is triggered by photolysis of the CO ligand.[46]) (B) Rotational diffusion times as a function of bulk viscosity for various concentrations of sucrose and dextran 70. The point where the dotted lines cross the sucrose line (310 mg/mL) corresponds to a sucrose viscosity equivalent to the microviscosity in a solution of 220 mg/mL dextran 70 (when the rotational diffusion time constants are equal, the microviscosities experienced by the protein are equal).

to the results of studies that have calculated microviscosity data from rotational and translational diffusion times measured with methods such as fluorescence correlation spectroscopy and time-resolved anisotropy.[12−15,40] Figure 4B shows that the sucrose concentration that gives the same rotational diffusion time as that found in 220 mg/mL dextran 70 is 310 mg/mL. Thus, these two conditions have the same microviscosity.

For oxcyt *c*, the near- and far-UV CD and MCD spectra reveal a similar unfolded state in 310 mg/mL sucrose as in buffer and in dextran 70 at 4 M GuHCl (Figures 1A,B and 2A). Similarly for redcyt *c*, the CD and MCD spectra (Figures 1A,C and 2B) show that secondary and tertiary structures and heme ligation in the presence of sucrose are similar to those of folded redcyt *c* (in NaP and dextran 70).

In Figure 3B, we compare the data for ET-triggered folding of redcyt *c* in the presence of 310 mg/mL sucrose with that previously measured in 4 M GuHCl and NaP. It is clear from the figure that the fast-folding phase (<1 ms) is present in the data measured in 4 M GuHCl, NaP, and 310 mg/mL sucrose, to an extent similar to that observed in buffer. We can thus conclude that the excluded volume effect and not increased

dx.doi.org/10.1021/bi301324y | *Biochemistry* 2012, 51, 9836−9845

viscosity is the reason for the diminished burst phase folding in dextran 70.

DISCUSSION

To understand protein folding reactions in vivo, the role of macromolecular crowding must be assessed. The effects of macromolecular crowding on kinetic processes will depend on both the length scale and the time scale involved. Here we study the folding reaction of reduced cyt *c* on the submillisecond time scale (corresponding to the burst phase of stopped-flow experiments). The kinetics of redcyt *c* folding in 220 mg/mL dextran 70, triggered by rapid electron transfer, was monitored by far-UV TRCD spectroscopy. The resulting TRCD data are compared to those measured previously without dextran 70.[34,36] To discriminate between the effects of excluded volume and changes in viscosity, TRCD measurements were also obtained for folding in the presence of 310 mg/mL sucrose, which provides the same microviscosity as dextran 70 but without excluded volume contributions. We find that the ultrafast folding step (<0.4 μs) observed in buffer[34,36] is significantly attenuated in the presence of dextran 70, suggesting that access to fast-folding conformations is reduced.

The decrease in the fast phase amplitude when redcyt *c* folds in the presence of dextran 70 suggests that there are structural and/or dynamic differences in the unfolded cyt *c* ensemble when crowding agents are present. However, equilibrium far- and near-UV CD and visible MCD measurements of unfolded oxcyt *c* suggest that there are no substantial structural differences. The fast-folding fraction of redcyt *c* molecules proceeds from a conformational ensemble that is kinetically isolated from the bulk of the unfolded-state conformers, i.e., kinetic partitioning.[34] The extent of equilibration of the unfolded conformers at the top of the folding funnel depends on conformational diffusion around the funnel. The conformational diffusion time constant for cyt *c* in NaP buffer is on the order of a few microseconds, similar to values reported for an ~100-residue polypeptide chain.[41] This conformational diffusion time means that folding processes occurring in microseconds will behave according to the landscape model, whereas folding processes occurring in hundreds of microseconds or more will follow classical kinetic mechanisms. The presence of dextran 70 may eliminate fast-folding molecules in two ways: by increasing the rate of conformational equilibration among unfolded conformers at the top of the folding funnel (allowing a faster equilibration time among unfolded conformers) or by altering the conformational space available to the unfolded polypeptides (so that the fast-folding subpopulation is not as populated). The first scenario implies that faster conformational equilibration would favor the slower folding ensembles and smooth the folding landscape during the early stages of folding. However, because the increased viscosity accompanying crowding should decrease rate constants related to conformational dynamics, and the sucrose sample with the same microviscosity as the sample with 220 mg/mL dextran 70 still exhibits fast folding, the second explanation (involving altered conformational space) appears more likely in the case of cyt *c* folding.

What may this "alteration of conformational space" be in molecular terms? The fast-folding population of redcyt *c* molecules found in dilute buffer was earlier proposed to be unfolded conformers with a His33−Fe−His18 heme configuration. This conclusion was based on comparative studies of horse redcyt *c* with tuna redcyt *c* (that naturally lacks His33) and a horse redcyt *c* mutant lacking both His33 and His26; both these variants do not display much fast formation of secondary structure.[42,43] On the basis of our observation described here, one may speculate that unfolded molecules with His33−Fe−His18 coordination (that are prone to fold fast) are eliminated in a crowded environment because of excluded volume effects. This could be the case if such bis-His conformers are more expanded in dimensions than other conformers. Time-resolved MCD experiments are currently in progress to investigate possible changes in the heme ligation state during early redcyt *c* folding upon the addition of dextran 70.

To assess unfolded-state dimensions with the two different bis-His heme ligations in silico, we used coarse-grained molecular simulations.[24,29] In these computations, the heme−Fe is permanently coordinated to His18 whereas His33 and His26 are allowed to interact with heme−Fe through nonpermanent interactions. In contrast to the speculation that His33−Fe−His18 coordination would not be favored under crowded conditions, we find that both bis-His heme coordinations are as likely to form in crowded environments as in buffer at very high temperatures ($T > 1.4\ k_BT/\varepsilon$, i.e., a highly denaturing condition) (Figure 5). However, there exists a

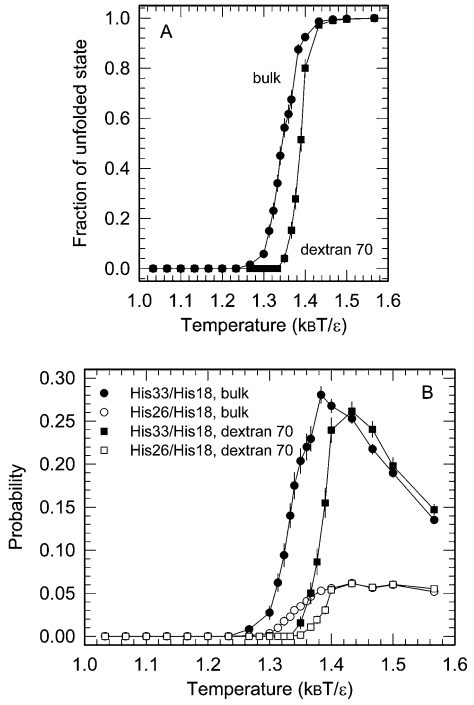

Figure 5. Coarse-grained simulations. (A) Fraction of molecules in the unfolded state as a function of temperature. (B) Probability of coordination between His26 and Fe−heme−His18 (and between His33 and Fe−heme−His18) as a function of temperature under bulk conditions and in the presence of dextran 70 at φ_c = 40% obtained from coarse-grained molecular simulations. Error bars are included.

significant difference in the size of the unfolded-state ensemble between crowded and noncrowded conditions. The unfolded ensemble is more compact in the presence of macromolecular crowding compared to that without crowding. This is evident for all unfolded conformations upon averaging (Figure 6A) as well as for the subpopulation of structures with the His33−Fe−His18 coordination (Figure 6B). Thus, it appears that under crowded conditions the unfolded ensemble is compacted, and

dx.doi.org/10.1021/bi301324y | *Biochemistry* 2012, 51, 9836−9845

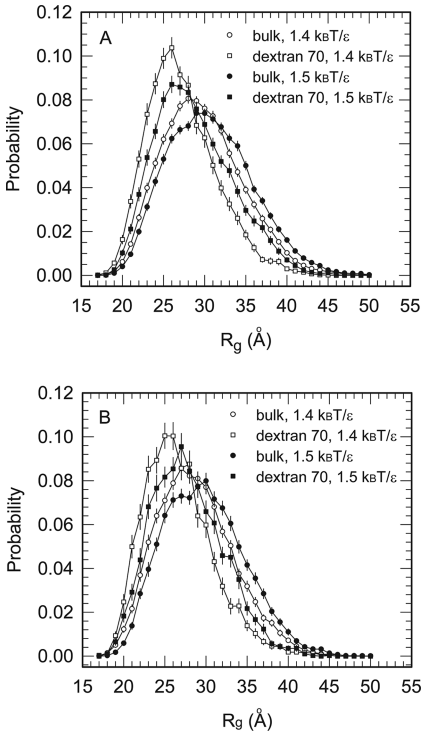

Figure 6. In silico distribution of radii of gyration of cyt *c* (A) in the ensemble of unfolded states (defined as $Q < 0.3$; Q is the fraction of native contacts) and (B) for conformations with His33−heme−His18 coordination selected out of the entire unfolded ensemble at 1.4 k_BT/ε and 1.5 k_BT/ε under bulk conditions and in the presence of dextran 70 at φ_c = 40%. Error bars are included.

this change in dimensions is not compatible with fast-folding conformers (regardless of specific His coordination). One possible structural explanation for this incompatibility is that formation of the fast-folding conformations requires movement through more expanded configurations. Thus, with structural compaction of the unfolded subpopulations, the slow folding path (U → N) is favored over fast folding via the molten globule intermediate.

Unfolded-state compaction in crowded environments is predicted from theory[6] and has been observed in coarse-grained simulations of several proteins, e.g., *Desulfovibrio desulfuricans* apoflavodoxin[10] and VlsE,[9] but there are only a few direct in vitro studies of this phenomenon. For *Azotobacter vinelandii* apoflavodoxin, FRET efficiency changes hinted that the presence of dextran 20 reduced the volume of the unfolded state.[44] Moreover, for the CRAB I protein, reduction of Trp and Cys probe accessibility was found for the unfolded state in the presence of Ficoll 70, suggesting a crowding-induced compaction of the unfolded state.[25]

Our TRCD observations can be compared to other kinetic experiments on protein folding in the presence of macromolecular crowding. According to fast fluorescence correlation spectroscopy studies of end-to-end contact formation in short peptides, 4−30 residues, rapid (nanosecond) formation of structural elements is not deterred by hindered diffusion in the presence of macromolecular crowding.[14] The authors suggested that reduction of the peptide chain entropy due to excluded volume effects in fact accelerated intrachain diffusion. In another study, nanosecond temperature-jump experiments with short peptides, which adopted specific folding motifs, in the presence of crowding agents also revealed that helix formation was not affected by crowding (although β-hairpins formed more slowly under crowded conditions).[15] Although different in terms of protein size and time scales studied, the results of these fluorescence studies support the idea arising from our TRCD studies that conformational equilibration kinetics within the unfolded cyt *c* ensemble is not affected by the presence of macromolecules. On longer time scales, a study of a set of point-mutated *Desulfovibrio vulgaris* apoflavodoxins found that in the presence of Ficoll 70, there was less initial (stopped-flow dead time of <1 ms) misfolding and the subsequent folding step (seconds) occurred faster than in buffer.[16] One explanation for these changes in apoflavodoxin folding was crowding-induced unfolded-state compaction. A reduced burst phase found in the stopped-flow experiments with apoflavodoxin is similar to the reduced amplitude of the fast folding step for redcyt *c* observed here under crowded conditions.

In conclusion, our study suggests that excluded volume effects due to macromolecular crowding compact the unfolded-state ensemble such that the access of cyt *c* to fast-folding conformations is decreased under crowded conditions. The loss of fast-folding conformers that are kinetically distinct from the bulk of the unfolded ensemble in the presence of crowding suggests smoothing of redcyt *c*'s folding landscape. Similar smoothing of the folding landscape was suggested in studies by Gruebele et al., in which a change from multistep folding in vitro to two-state folding inside living cells was demonstrated for the protein phosphoglycerate kinase.[17] Finally, we note that in vivo, weak, transient protein−protein interactions may also play a role, as recently demonstrated by in-cell NMR.[45]

AUTHOR INFORMATION

Corresponding Author

*P.W.-S.: phone, +46-90-7865347; fax, +46-90-7867655; e-mail, pernilla.wittung@chem.umu.se. D.S.K.: phone, (831) 459-2106; fax, (831) 459-2935; e-mail, kliger@ucsc.edu.

Funding

We thank the Swedish Natural Research Council (P.W.-S.), the Knut and Alice Wallenberg Foundation (P.W.-S.), the Göran Gustafsson Foundation (P.W.-S.), the J. C. Kempe Foundation (P.W.-S.), and Umeå University Young Researcher Awards (P.W.-S.) for financial support. Q.W. and M.S.C. thank the National Science Foundation (MCB0919974) for financial support and the Research Computing Center and the Texas Learning and Computational Center at the University of Houston for computational resources.

Notes

The authors declare no competing financial interest.

ABBREVIATIONS

cyt *c*, cytochrome *c*; oxcyt *c*, oxidized cytochrome *c*; redcyt *c*, reduced cytochrome *c*; TRCD, time-resolved circular dichroism; TRLD, time-resolved linear dichroism; TROD, time-resolved absorption; TRORD, time-resolved optical rotatory dispersion; GuHCl, guanidinium hydrochloride; ET, electron transfer; MbCO, carbon monoxy-bound myoglobin; MCD, magnetic circular dichroism.

REFERENCES

(1) Matouschek, A., Kellis, J. T., Jr., Serrano, L., and Fersht, A. R. (1989) Mapping the transition state and pathway of protein folding by protein engineering. *Nature 340*, 122−126 (see comments).

(2) Bryngelson, J. D., Onuchic, J. N., Socci, N. D., and Wolynes, P. G. (1995) Funnels, pathways, and the energy landscape of protein folding: A synthesis. *Proteins 21*, 167−195.
(3) Rivas, G., Ferrone, F., and Herzfeld, J. (2004) Life in a crowded world. *EMBO Rep. 5*, 23−27.
(4) Ellis, R. J., and Minton, A. P. (2003) Cell biology: Join the crowd. *Nature 425*, 27−28.
(5) Laurent, T. C., and Ogston, A. G. (1963) The Interaction between Polysaccharides and Other Macromolecules. 4. The Osmotic Pressure of Mixtures of Serum Albumin and Hyaluronic Acid. *Biochem. J. 89*, 249−253.
(6) Minton, A. P. (2005) Models for excluded volume interaction between an unfolded protein and rigid macromolecular cosolutes: Macromolecular crowding and protein stability revisited. *Biophys. J. 88*, 971−985.
(7) Zhou, H. X. (2004) Loops, linkages, rings, catenanes, cages, and crowders: Entropy based strategies for stabilizing proteins. *Acc. Chem. Res. 37*, 123−130.
(8) Cheung, M. S., Klimov, D., and Thirumalai, D. (2005) Molecular crowding enhances native state stability and refolding rates of globular proteins. *Proc. Natl. Acad. Sci. U.S.A. 102*, 4753−4758.
(9) Homouz, D., Perham, M., Samiotakis, A., Cheung, M. S., and Wittung-Stafshede, P. (2008) Crowded, cell-like environment induces shape changes in aspherical protein. *Proc. Natl. Acad. Sci. U.S.A. 105*, 11754−11759.
(10) Stagg, L., Zhang, S. Q., Cheung, M. S., and Wittung-Stafshede, P. (2007) Molecular crowding enhances native structure and stability of α/β protein flavodoxin. *Proc. Natl. Acad. Sci. U.S.A. 104*, 18976−18981.
(11) Sasahara, K., McPhie, P., and Minton, A. P. (2003) Effect of dextran on protein stability and conformation attributed to macromolecular crowding. *J. Mol. Biol. 326*, 1227−1237.
(12) Lavalette, D., Hink, M. A., Tourbez, M., Tetreau, C., and Visser, A. J. (2006) Proteins as micro viscosimeters: Brownian motion revisited. *Eur. Biophys. J. 35*, 517−522.
(13) Lavalette, D., Tetreau, C., Tourbez, M., and Blouquit, Y. (1999) Microscopic viscosity and rotational diffusion of proteins in a macromolecular environment. *Biophys. J. 76*, 2744−2751.
(14) Neuweiler, H., Lollmann, M., Doose, S., and Sauer, M. (2007) Dynamics of unfolded polypeptide chains in crowded environment studied by fluorescence correlation spectroscopy. *J. Mol. Biol. 365*, 856−869.
(15) Mukherjee, S., Waegele, M. M., Chowdhury, P., Guo, L., and Gai, F. (2009) Effect of macromolecular crowding on protein folding dynamics at the secondary structure level. *J. Mol. Biol. 393*, 227−236.
(16) Stagg, L., Christiansen, A., and Wittung-Stafshede, P. (2011) Macromolecular crowding tunes folding landscape of parallel α/β protein, apoflavodoxin. *J. Am. Chem. Soc. 133*, 646−648.
(17) Dhar, A., Girdhar, K., Singh, D., Gelman, H., Ebbinghaus, S., and Gruebele, M. (2011) Protein stability and folding kinetics in the nucleus and endoplasmic reticulum of eucaryotic cells. *Biophys. J. 101*, 421−430.
(18) Lewis, J. W., Tilton, R. F., Einterz, C. M., Milder, S. J., Kuntz, I. D., and Kliger, D. S. (1985) New technique for measuring circular dichroism changes on a nanosecond time scale: Application to (carbonmonoxy)myoglobin and (carbonmonoxy)hemoglobin. *J. Phys. Chem. 89*, 289−294.
(19) Kliger, D. S., Chen, E., and Goldbeck, R. A. (2012) Nanosecond time-resolved natural and magnetic chiroptical spectroscopies. *Instrumentation, Methodologies and Theoretical Simulations*, Vol. *1*, Wiley-VCH, New York.
(20) Goldbeck, R. A., Chen, E., and Kliger, D. S. (2009) Early events, kinetic intermediates and the mechanism of protein folding in cytochrome *c*. *Int. J. Mol. Sci. 10*, 1476−1499.
(21) Keilin, D. (1966) *The history of cell respiration and cytochrome*, Cambridge University Press, Cambridge, U.K.
(22) Liu, X., Kim, C. N., Yang, J., Jemmerson, R., and Wang, X. (1996) Induction of apoptotic program in cell-free extracts: Requirement for dATP and cytochrome *c*. *Cell 86*, 147−157.
(23) Che, D. P., Shapiro, D. B., Esquerra, R. M., and Kliger, D. S. (1994) Ultrasensitive Time-Resolved Linear Dichroism Spectral Measurements Using near-Crossed Linear Polarizers. *Chem. Phys. Lett. 224*, 145−154.
(24) Christiansen, A., Wang, Q., Samiotakis, A., Cheung, M. S., and Wittung-Stafshede, P. (2010) Factors defining effects of macromolecular crowding on protein stability: An in vitro/in silico case study using cytochrome *c*. *Biochemistry 49*, 6519−6530.
(25) Hong, J., and Gierasch, L. M. (2010) Macromolecular crowding remodels the energy landscape of a protein by favoring a more compact unfolded state. *J. Am. Chem. Soc. 132*, 10445−10452.
(26) Vickery, L., Nozawa, T., and Sauer, K. (1976) Magnetic circular dichroism studies of low-spin cytochromes. Temperature dependence and effects of axial coordination on the spectra of cytochrome *c* and cytochrome b_5. *J. Am. Chem. Soc. 98*, 351−357.
(27) O'Connor, D. B., Goldbeck, R. A., Hazzard, J. H., Kliger, D. S., and Cusanovich, M. A. (1993) Time-resolved absorption and magnetic circular dichroism spectroscopy of cytochrome c_3 from *Desulfovibrio*. *Biophys. J. 65*, 1718−1726.
(28) Cheung, M. S., Finke, J. M., Callahan, B., and Onuchic, J. N. (2003) Exploring the interplay between topology and secondary structural formation in the protein folding problem. *J. Phys. Chem. B 107*, 11193−11200.
(29) Weinkam, P., Zong, C., and Wolynes, P. G. (2005) A funneled energy landscape for cytochrome *c* directly predicts the sequential folding route inferred from hydrogen exchange experiments. *Proc. Natl. Acad. Sci. U.S.A. 102*, 12401−12406.
(30) Veitshans, T., Klimov, D., and Thirumalai, D. (1997) Protein folding kinetics: Timescales, pathways and energy landscapes in terms of sequence-dependent properties. *Folding Des. 2*, 1−22.
(31) Sugita, Y., and Okamoto, Y. (1999) Replica-exchange molecular dynamics method for protein folding. *Chem. Phys. Lett. 314*, 141−151.
(32) Mines, G. A., Pascher, T., Lee, S. C., Winkler, J. R., and Gray, H. B. (1996) Cytochrome *c* folding triggered by electron transfer. *Chem. Biol. 3*, 491−497.
(33) Pascher, T., Chesick, J. P., Winkler, J. R., and Gray, H. B. (1996) Protein folding triggered by electron transfer. *Science 271*, 1558−1560.
(34) Chen, E. F., Goldbeck, R. A., and Kliger, D. S. (2003) Earliest events in protein folding: Submicrosecond secondary structure formation in reduced cytochrome *c*. *J. Phys. Chem. A 107*, 8149−8155.
(35) Zhou, H. X., Rivas, G., and Minton, A. P. (2008) Macromolecular crowding and confinement: Biochemical, biophysical, and potential physiological consequences. *Annu. Rev. Biophys. 37*, 375−397 (and references cited therein).
(36) Chen, E. F., Wittung-Stafshede, P., and Kliger, D. S. (1999) Far-UV time-resolved circular dichroism detection of electron-transfer-triggered cytochrome *c* folding. *J. Am. Chem. Soc. 121*, 3811−3817.
(37) Lee, J. C., Gray, H. B., and Winkler, J. R. (2001) Cytochrome c′ folding triggered by electron transfer: Fast and slow formation of four-helix bundles. *Proc. Natl. Acad. Sci. U.S.A. 98*, 7760−7764.
(38) Chen, E., Van Vranken, V., and Kliger, D. S. (2008) The folding kinetics of the SDS-induced molten globule form of reduced cytochrome *c*. *Biochemistry 47*, 5450−5459.
(39) Shastry, M. C., and Roder, H. (1998) Evidence for barrier-limited protein folding kinetics on the microsecond time scale. *Nat. Struct. Biol. 5*, 385−392.
(40) Goins, A. B., Sanabria, H., and Waxham, M. N. (2008) Macromolecular crowding and size effects on probe microviscosity. *Biophys. J. 95*, 5362−5373.
(41) Abel, C. J., Goldbeck, R. A., Latypov, R. F., Roder, H., and Kliger, D. S. (2007) Conformational equilibration time of unfolded protein chains and the folding speed limit. *Biochemistry 46*, 4090−4099 (and references cited therein).
(42) Chen, E. F., Goldbeck, R. A., and Kliger, D. S. (2004) The earliest events in protein folding: A structural requirement for ultrafast folding in cytochrome *c*. *J. Am. Chem. Soc. 126*, 11175−11181.
(43) Chen, E., Abel, C. J., Goldbeck, R. A., and Kliger, D. S. (2007) Non-native heme-histidine ligation promotes microsecond time scale

secondary structure formation in reduced horse heart cytochrome *c*. *Biochemistry 46*, 12463−12472.
(44) Engel, R., Westphal, A. H., Huberts, D. H., Nabuurs, S. M., Lindhoud, S., Visser, A. J., and van Mierlo, C. P. (2008) Macromolecular crowding compacts unfolded apoflavodoxin and causes severe aggregation of the off-pathway intermediate during apoflavodoxin folding. *J. Biol. Chem. 283*, 27383−27394.
(45) Wang, Q., Zhuravleva, A., and Gierasch, L. M. (2011) Exploring weak, transient protein−protein interactions in crowded in vivo environments by in-cell nuclear magnetic resonance spectroscopy. *Biochemistry 50*, 9225−9236.
(46) Chen, E. F., Wood, M. J., Fink, A. L., and Kliger, D. S. (1998) Time-resolved circular dichroism studies of protein folding intermediates of cytochrome *c*. *Biochemistry 37*, 5589−5598.